chemistry proceedings

MDPI

Proceeding Paper

Synthesis and Characterization of 3D Nanoporous Copper Oxide Materials by Dealloying and Thermal Oxidation of Amorphous Ribbons

Mircea Nicolaescua[1,2], Cosmin Codrean[2], Corina Orha[1] and Cornelia Bandas[1*]

[1]National Institute for Research and Development in Electrochemistry and Condensed Matter, A. Paunescu Podeanu Street, No 144, Timisoara 300569, Romania; cornelia.bandas@gmail.com (C.B); orha.corina@gmail.com (C.O.);
[2]Politehnica University Timisoara, P-ta Victoriei, No. 2, Timisoara 300006, Romania; nicolaescu.mircea13@yahoo.com (M.N.); cosmin.codrean@upt.ro (C.C.)
* Correspondence: cornelia.bandas@gmail.com.

Abstract: A nanoporous copper oxide (NP-CuO) materials synthesized by dealloying and thermal oxidation of amorphous CuZrAl ribbons, representing the novelty of this research, previously obtained by a melt-spinning process, was carried out in an aqueous hydrofluoric acid (HF) solution by varying the holding time. These nanoporous copper (NPC) structures are used as a template to achieve a 3D-NP-CuO material with different surface morphology. To investigate the structural and morphological properties of the obtained sandwich-type material, X-ray diffraction (XRD), scanning electron microscopy coupled with energy dispersive x-ray spectroscopy (SEM/EDX), and ultraviolet-visible spectroscopy (UV-VIS) were used. In summary, the dealloying and thermal oxidation of amorphous ribbons is an interesting approach to achieve a three-dimensional (3D) network of NP-CuO with different morphologies and with a low production cost. These sandwich-type structures consisting of NPC and copper oxide nanowires (CuO/Cu_2O), combines the good electrical properties of NPC with the catalytic properties of copper oxide semiconductors making it a suitable material for photocatalysis, photoelectrodes in solar cells, battery applications and electrochemical sensors.

Keywords: Amorphous ribbons; Dealloying; Thermal Oxidation; Nanoporous Copper Oxide; Nanowires

Citation: To be added by editorial staff during production.

Academic Editor: Firstname Lastname

Published: date

1. Introduction

Metal oxide semiconductors are very attractive materials for industries with particularity for the energy conversion sector, sensor industry, and environment remediation industry [1-3]. Copper has two oxidation state oxides, cupric oxide (CuO) and cuprous oxide (Cu_2O), both having semiconductor properties with band gaps of 1.2 and 2.0 eV, respectively. Their energy band gaps make them a good candidate for solar cells, water splitting devices, and sensor devices [1,4]. Nanoporous materials are an important class of functional materials that improve the propriety because of the large surface area and their surface-to-weight ratio [5]. Dealloying process is one of the routes to produce nanoporous and microporous materials by selective dissolution of less noble elements in acidic or basic solution [6,7]. Amorphous ribbons have a homogeneous composition and, compared to crystalline alloys, do not have grain boundaries or defects, making them an ideal candidate for the dealloying process [8]. Through the dealloying process using amorphous materials nanoporous gold (NPG) [9], nanoporous silver (NPS) [10], nanoporous platinum (NPP) [11], nanoporous nickel (NPN) [12], and nanoporous copper (NPC) [13] were synthesized, as well as other nanoporous composite materials (metal-metal or metal-oxide) [14,15].

The synthesis of NPCs by dealloying has been studied by groups of researchers around the world in bulk or ribbon form, from various amorphous alloy systems. *Dan et al.*, produce the NPC structure from TixCu100x amorphous binary alloys (x = 40, 50 and 60%.) in hydrofluoric acid solution under free corrosion conditions. The tapes that were dealloyed in HF solution with a concentration of 0.03 M show a bicontinuous nanoporous structure having a pore size of 25 to 75 nm and a ligament size of 46 to 79 nm. The dealloyed ribbons in 0.13 M HF solution have a pore size of 85-380 nm and a ligament size of 80-338 nm [8].

Li et al. presented a relatively simple two-step synthesis method (dealloying - electrochemical oxidation) to produce Cu_2O / CuO nanoporous oxide heterostructures, using massive amorphous metal rods (BMG). The NPC was manufactured by chemically dealloying the bulk alloy rod $Cu_{50}Zr_{45}Al_5$ (BMG) in 0.05M HF at 298 K for 1 day. The growth of CuO and Cu_2O heterostructures was carried out electrochemically at a temperature of 298 K in 0.5 M KOH and at a constant current density of 5 mA cm^{-2} for 10-30 min [15].

Thermal oxidation is one of the simplest processes to produce a wide range of micro and nano-oxide structures such as nanowires, nanoflakes, and nanoneedles on the metal surface [16—18]. This process involves heating metal substrates, such as foil, plates, and wires, in the presence of air. Amorphous ribbons from the CuZr systems have been widely used as dealloying alloys and as-nanostructured oxides for various applications. Zr and Al standard equilibrium potentials are larger than those for Cu [4, 19]. The difference in the standard electrode potentials between these elements means that the Cu–Zr-Al amorphous alloy meets the requirements for dealloying.

In the present work, NPC substrate produced by the free dealloying process of CuZrAl ribbons was used as a template to obtain nanoporous copper oxide by thermal oxidation process. The influence of holding time at temperature of 500 ° C on the surface morphology was also discussed.

2. Materials and Methods

2.1. Preparation of amorphous ribbons

To produce an amorphizable alloy with the nominal composition of $Cu_{48}Zr_{47}Al_5$, the arc melting process was used with a mixture of pure Cu (99.99 wt%), pure Zr (99.9 wt%) and Al (99.9 wt%) in an Ar atmosphere. The CuZrAl amorphous ribbon was prepared by the melt-spinning method. As-produced ribbons have a thickness of 20 μm and a width of 2 mm. The dealloying process was carried out in a 0.5 M HF solution, purchased from Sigma-Aldrich Company (St. Louis, MO, USA) under free immersion at room temperature for a reaction time of 2 hours. After corrosion, the ribbons were washed with distilled water to remove any residual HF solution.

2.2. Thermal oxidation process

The thermal oxidation of the prepared nanoporous ribbons was carried out at 500 °C for 6, 12 and 24 hours in air atmosphere. The heating rate (10 ° C / min) was maintained until the oxidation temperatures were reached.

2.33. D-NP-CuO material characterization

To study the structure of the Cu-Zr-Al ribbons, before and after dealloying, and also after the thermal oxidation, X-ray diffraction (XRD) patterns were collected using a PANalytical X'Pert PRO MPD diffractometer with Cu-Kα radiation with (λ=1.5418Å), in the range of 2θ = 10-80° from Almelo, Netherlands. The surface morphology of the samples obtained before and after thermal oxidation was examined by scanning electron microscopy (SEM) using an Inspect S + EDAX GENESIS XM 2i microscope from FEI Company from Eindhoven, Netherlands. Energy-dispersive X-ray spectroscopy using an EDX Ametek Element Module was used for elemental identification of the samples from Eindhoven, Netherlands. The optical properties of the material were recorded using UV-Vis

analysis PerkinElmer Lambda 950 UV/Vis spectrophotometer, in the range of 350–800 nm from Connecticut, USA. The band gap Eg of the materials was determined by plotting the Kubelka–Munk function against energy (eV).

3. Results and Discussion

The XRD patterns of the amorphous and dealloyed ribbons are illustrated in Figure 1a. A broad intensity peak appeared in the XRD diffraction patterns of the amorphous ribbons at an 2θ angle in the range of 35°–45°, which is reflecting the amorphous state of the CuZrAl alloy. After the dealloying process, the most electrochemically active elements (Zr and Al) were selective removed. The nonporous metal is composed primordially of face-centered cubic (fcc) Cu (JCPDS card No. 00-004-0836) and some cubic Cu_2O (JCPDS card No. 01-078-2076). The Cu_2O nanoparticle is obtained on the NPC substrate, probably because the dealloying method was carried out in an oxygen-rich corrosive solution, resulting in some of the copper atoms of the NPC react with the dissolved oxygen, resulting in Cu_2O nanoparticles [20]. In Figure 1b is presented XRD patterns of the as-synthesized 3D-NP-CuO material, after thermal oxidation. Due to the high surface area of the NPC ribbons after thermal oxidation, copper atoms react with the oxygen in the atmosphere and the sample becomes primordially composed of monoclinic CuO (JCPDS card No. 00-005-0661) for all thermal oxidation parameters. Based on XRD results and according to literature data, it can be concluded that the formation process of the produced CuO nanoparticles and nanowires includes two reaction steps [21]:

$$4Cu + O_2 \rightarrow Cu_2O\ ; \quad (1)$$

$$2Cu_2O + O_2 \rightarrow CuO; \quad (2)$$

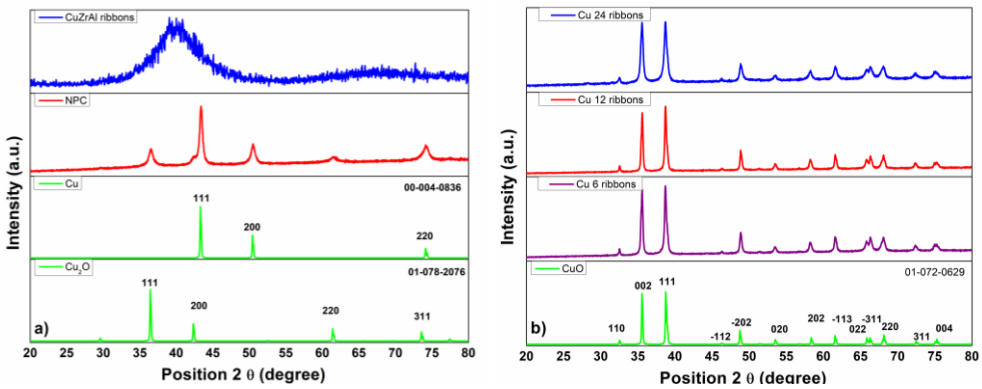

Figure 1. XRD pattern of copper base amorphous ribbons for **(a)** amorphous and nanoporous cooper and **(b)** 3D-NP-CuO material.

Figure 2 shows the surface morphology of the as-dealloyed CuZrAl amorphous ribbons in a 0.5 M HF solution at room temperature at 2 hours of holding time. The pores size was measured from SEM images using ImageJ software and defined as the distance between the ligaments / particles. The dealloyed $Cu_{48}Zr_{47}Al_5$ amorphous ribbon presents a 3D bicontinuous nonporous structure with an average length ligament at 26.75 nm. This structure resulted from the rearrangement of the copper atom after zirconium and aluminum were removed. The Cu_2O structure shown in the XRD pattern (Figure 1a) is not clearly highlighted in the SEM image (Figure 2a) possibly due to the nanosize of the Cu_2O particles. In Figures 2b, c, d, the samples with different surface morphologies synthesized through the thermal oxidation process are presented.

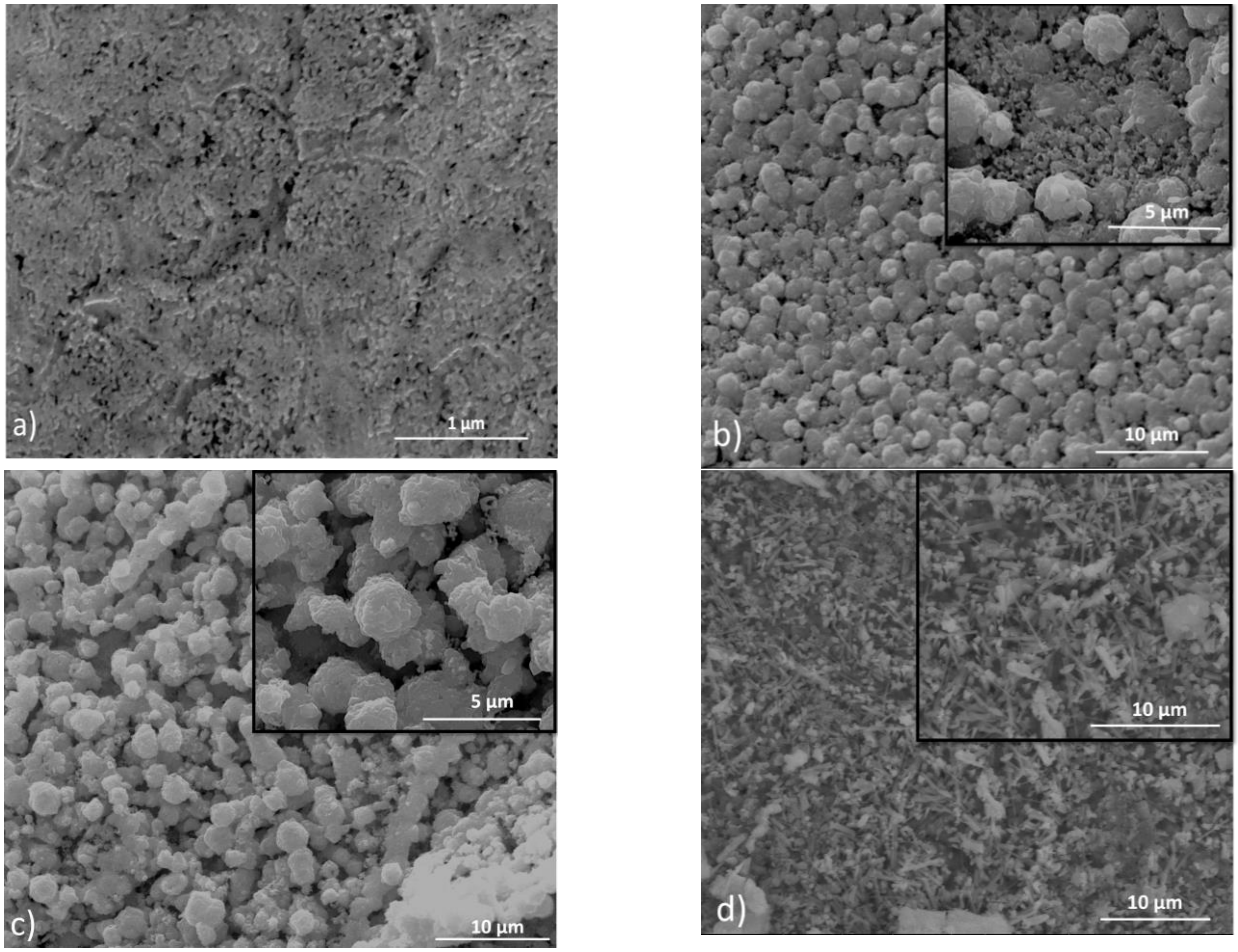

Figure 2. SEM morphologies of the NPC and NP-CuO samples for **(a)** NPC; **(b)** NP-CuO obtained at 500 °C for a holding time of 6 h; **(c)** NP-CuO obtained at 500 °C for a holding time of 12h; **(d**) NP-CuO obtained at 500 °C for a holding time of 24 h.

Figure 2b shows the SEM images of the thermal oxidation sample at 500 °C for a holding time of 6 hours. It can be seen that the synthesized monoclinic CuO material presents a homogeneous distributed 3D interconnected sphere, which are composed of many nanorods. The 3D copper oxide nanoparticles show a nanopore structure mimicking the NPC template [22]. From the inset of the Figure 2b, it can be seen that the larger spheres are formed on a 3D substrate compound from smaller interconnected nanorods and much smaller nanospheres. The average length of the surface sphere was 1.63 µm and the average distance between them was about 505 nm. The distance between the 3D substrates was about 152 nm. Figure 2c presents the SEM image of the sample obtained at 12 hours holding time. The 3D interconnected spheres of the CuO material have an increase in surface oxidation and porosity, and the larger spheres are in average at 160 µm and the average distance between particles was 936 nm. In Figure 2d, due to the increase of the holding time at 24 hours on the surface of 3D CuO material, the in-situ growth of CuO nanowires continues having the average length of 196 nm. The nanowires are randomly distributed on the 3D CuO surface, further increasing the surface-to-volume ratio.

The typical EDX spectra shown in Figure 3, confirmed the complete dealloying of Zr and Al atoms from the amorphous ribbons. Due to the diffusion of oxygen from the dealloying process and the natural oxidation of the nanoporous ribbons, the oxygen element was presented in Figure 3a. Figures 3 b, c and d present the increase of oxygen content after thermal oxidation and the presence of the single metal element (Cu). A site increase of the O atom is shown in Figure 3d, due to the oxide nanowire on the NP-CuO surface.

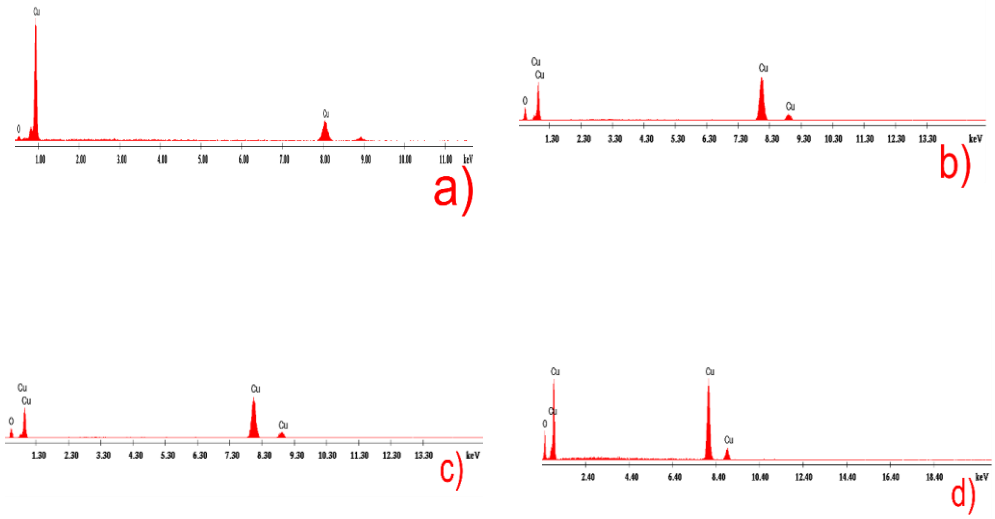

Figure 3. EDX spectrum of NPC and NP-CuO samples for **(a)** NPC; **(b)** NP-CuO obtained at 500 ° C for 6 h holding time; **(c)** NP-CuO obtained at 500 ° C for 12 h holding time; **(d)** NP-CuO obtained at 500 ° C for 24 h holding time.

The UV-vis absorption spectra of the synthesized NP-CuO were shown in Figure 4a. The absorption spectra present a very high absorption in both the visible region and the UV region, this fact being probably generated by the nanoporous oxide structure [23]. The optical band gaps of NP-CuO materials were determined using the Tauc plot method, using the following equation 3 [24]:

$$\alpha hm = A(h\upsilon - Eg)^n \quad (3)$$

where α is the absorption coefficient, hv is the photon energy, A is a proportionality constant, and Eg is the optical band gap.

The p-type CuO semiconductors have reported optical band gaps between 1.3 and 2.1 eV [25]. In our study, for the NP-CuO samples a high bandgap at 3.68 eV was reported for the surface nanowire sample. For the sample oxidized for 6 and 12 h, a band gap at 3.58 and 3.30 eV, respectively, was presented. A slight increase in the band for the material synthesized for 24 h was due to the unidimensional structure on the NP-CuO surface. A blue shift was indicated from our results, generate by the reduce particle size. This blue shift has been reported in the literature for CuO quantum dots, because of the quantum confinement effects [26,27].

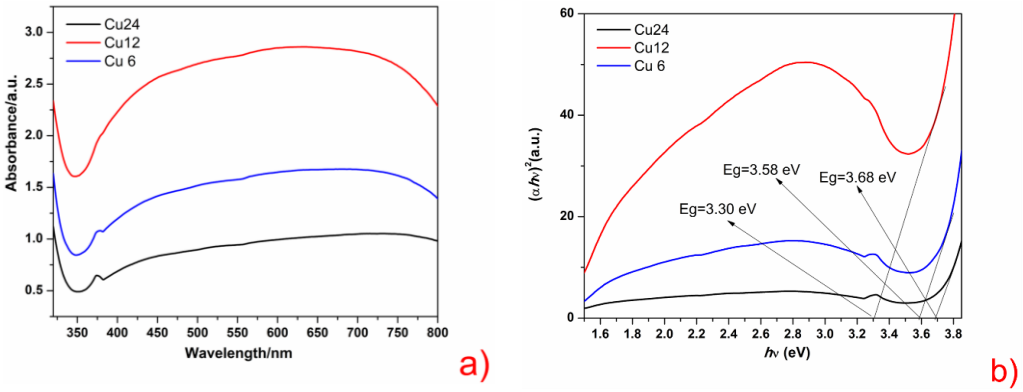

Figure 4. (a) Absorption spectra and **(b)** Band-gap values of the as-synthesized samples at different temperatures.

5. Conclusions

In summary, the dealloying and thermal oxidation of amorphous ribbons is an interesting approach to achieve 3D networks of NP-CuO with different morphologies and with a low production cost. The absorption spectra of NP-CuO samples show a wide absorption band in the 350–800 nm region and a high surface to volume ratio which can lead to an enhanced photocatalytic activity for environmental remediation. Because of the wide absorption spectra, NP-CuO might be used as an ideal harvester for solar irradiation. At an increased holding time of 24 h, on the surface of NP-CuO, successfully unidimensional nanowires are synthesized. For the first time in this work, a high energy band gap value in the range of 3.30 eV and 3.68 eV was reported for the CuO nanoparticles obtained by the dealloying and thermal oxidation of amorphous ribbons.

Author Contributions: M.N. was involved in conceptualization, methodology, investigation, writing—original draft; C.C. was involved in conceptualization, methodology, investigation, writing—original draft; C.O. was involved in conceptualization, methodology, investigation, writing—original draft; C.B. was involved in methodology, investigation, writing—original draft, supervision. All authors have read and agreed to the published version of the manuscript.

Funding: This work was supported by a grant of the Ministry of Research, Innovation and Digitization, CNCS - UEFISCDI, project number PN-III-P1-1.1-TE-2021-0963, within PNCDI III, with contract number TE13/2022 (DD-CyT); by Project "Network of excellence in applied research and innovation for doctoral and postdoctoral programs / InoHubDoc", project co-funded by the European Social Fund financing agreement no. POCU/993/6/13/153437, and partially by project code PN 23 27 01 02 INOMAT, 23-27 29N/2023.

Institutional Review Board Statement: Not applicable.

Informed Consent Statement: Not applicable.

Data Availability Statement: Not applicable.

Conflicts of Interest: The authors declare no conflict of interest.

References

1. Vajda, M.; Ursu, D.; Miclau, N.; Duteanu, N.; Miclau, M. Fabrication of copper oxide-based dye-sensitized solar cell with high short-circuit current density (JSC) using flexible and binder-free porous photoelectrode. Journal of Materials Science: Materials in Electronics 2022, 33, doi:10.1007/s10854-022-08888-1.
2. Liu, D.; Yang, Z.; Wang, P.; Li, F.; Wang, D.; He, D. Preparation of 3D nanoporous copper-supported cuprous oxide for high-performance lithium ion battery anodes. Nanoscale 2013, 5, 1917-1921, doi:10.1039/c2nr33383j.
3. Liu, X.; Du, J.; Shao, Y.; Zhao, S.F.; Yao, K.F. One-pot preparation of nanoporous Ag-Cu@Ag core-shell alloy with enhanced oxidative stability and robust antibacterial activity. Sci Rep 2017, 7, 10249, doi:10.1038/s41598-017-10630-5.
4. Zhou, M.; Huang, X.; Hagos, K.; Cui, Y.; Ma, L. Nanoporous copper fabricated from Zr 65 Cu 17.5 Fe 10 Al 7.5 amorphous alloy and its electrocatalytic oxidation performance. Intermetallics 2017, 90, 23-29, doi:10.1016/j.intermet.2017.06.005.
5. Wang, Y.M.; Zhang, W.; Inoue, A. Nanoporous Cu wide ribbons with good mechanical integrity. Materials Science and Engineering: B 2012, 177, 532-535, doi:10.1016/j.mseb.2011.12.025.
6. McCue, I.; Benn, E.; Gaskey, B.; Erlebacher, J. Dealloying and Dealloyed Materials. Annual Review of Materials Research 2016, 46, 263-286, doi:10.1146/annurev-matsci-070115-031739.
7. An, Y.; Tian, Y.; Wei, C.; Tao, Y.; Xi, B.; Xiong, S.; Feng, J.; Qian, Y. Dealloying: An effective method for scalable fabrication of 0D, 1D, 2D, 3D materials and its application in energy storage. Nano Today 2021, 37, 101094, doi:10.1016/j.nantod.2021.101094.
8. Dan, Z.; Qin, F.; Yamaura, S.-i.; Sugawara, Y.; Muto, I.; Hara, N. Dealloying behavior of amorphous binary Ti–Cu alloys in hydrofluoric acid solutions at various temperatures. Journal of Alloys and Compounds 2013, 581, 567-572, doi:10.1016/j.jallcom.2013.07.144.

9. Chao, B.K.; Xu, Y.; Ho, H.C.; Yiu, P.; Lai, Y.C.; Shek, C.H.; Hsueh, C.H. Gold-rich ligament nanostructure by dealloying Au-based metallic glass ribbon for surface-enhanced Raman scattering. Sci Rep 2017, 7, 7485, doi:10.1038/s41598-017-08033-7.
10. Jin, Y.; Li, R.; Zhang, T. Formation of nanoporous silver by dealloying Ca–Ag metallic glasses in water. Intermetallics 2015, 67, 166-170, doi:10.1016/j.intermet.2015.08.011.
11. Wang, S.; Li, H.; Lin, H.; Wu, K. Enhanced electro-catalytic performance of Pd-based hierarchical nanoporous structures fabricated by micropatterning and dealloying of Pd-Ni-P metallic glass. Nanotechnology 2020, 31, 155301, doi:10.1088/1361-6528/ab667f.
12. Zheng, D.; Zhao, F.; Li, Y.; Qin, C.; Zhu, J.; Hu, Q.; Wang, Z.; Inoue, A. Flexible NiO micro-rods/nanoporous Ni/metallic glass electrode with sandwich structure for high performance supercapacitors. Electrochimica Acta 2019, 297, 767-777, doi:10.1016/j.electacta.2018.12.035.
13. Wang, Z.; Liu, J.; Qin, C.; Liu, L.; Zhao, W.; Inoue, A. Fabrication and new electrochemical properties of nanoporous Cu by dealloying amorphous Cu–Hf–Al alloys. Intermetallics 2015, 56, 48-55, doi:10.1016/j.intermet.2014.09.002.
14. Dan, Z.; Qin, F.; Makino, A.; Sugawara, Y.; Muto, I.; Hara, N. Fabrication of nanoporous copper by dealloying of amorphous Ti–Cu–Ag alloys. Journal of Alloys and Compounds 2014, 586, S134-S138, doi:10.1016/j.jallcom.2013.01.087.
15. Li, M.; Li, Y.; Zhang, Q.; Qin, C.; Zhao, W.; Wang, Z.; Inoue, A. Ultrafine Cu2O/CuO nanosheet arrays integrated with NPC/BMG composite rod for photocatalytic degradation. Applied Surface Science 2019, 483, 285-293, doi:10.1016/j.apsusc.2019.03.313.
16. Filipic, G.; Cvelbar, U. Copper oxide nanowires: a review of growth. Nanotechnology 2012, 23, 194001, doi:10.1088/0957-4484/23/19/194001.
17. Li, A.; Song, H.; Wan, W.; Zhou, J.; Chen, X. Copper oxide nanowire arrays synthesized by in-situ thermal oxidation as an anode material for lithium-ion batteries. Electrochimica Acta 2014, 132, 42-48, doi:10.1016/j.electacta.2014.03.123.
18. Nicolaescu, M.; Orha, C.; Dabici, A.; Hididis, P.; Codrean, C.; Șerban, V.A. Production of Cu-Zr mixed metal oxides by thermal oxidation of amorphous ribbons. Materials Today: Proceedings 2021, 45, 4337-4343, doi:10.1016/j.matpr.2020.12.1157.
19. Lu, H.-B.; Li, Y.; Wang, F.-H. Synthesis of porous copper from nanocrystalline two-phase Cu–Zr film by dealloying. Scripta Materialia 2007, 56, 165-168, doi:10.1016/j.scriptamat.2006.09.009.
20. Wang, Z.; Liu, J.; Qin, C.; Yu, H.; Xia, X.; Wang, C.; Zhang, Y.; Hu, Q.; Zhao, W. Dealloying of Cu-Based Metallic Glasses in Acidic Solutions: Products and Energy Storage Applications. Nanomaterials (Basel) 2015, 5, 697-721, doi:10.3390/nano5020697.
21. Zhu, D.; Wang, L.; Yu, W.; Xie, H. Intriguingly high thermal conductivity increment for CuO nanowires contained nanofluids with low viscosity. Sci Rep 2018, 8, 5282, doi:10.1038/s41598-018-23174-z.
22. Sasikala, N.T.; Boominathasellarajan, S.; Raghupathy, B.P.C. Fabrication of Nanostructures Using Porous Anodic Alumina Template. International Journal of Nanoscience 2012, 10, 783-786, doi:10.1142/s0219581x11008897.
23. Bin Mobarak, M.; Hossain, M.S.; Chowdhury, F.; Ahmed, S. Synthesis and characterization of CuO nanoparticles utilizing waste fish scale and exploitation of XRD peak profile analysis for approximating the structural parameters. Arabian Journal of Chemistry 2022, 15, 104117, doi:10.1016/j.arabjc.2022.104117.
24. Makula, P.; Pacia, M.; Macyk, W. How To Correctly Determine the Band Gap Energy of Modified Semiconductor Photocatalysts Based on UV-Vis Spectra. J Phys Chem Lett 2018, 9, 6814-6817, doi:10.1021/acs.jpclett.8b02892.
25. Murali, D.S.; Kumar, S.; Choudhary, R.J.; Wadikar, A.D.; Jain, M.K.; Subrahmanyam, A. Synthesis of Cu2O from CuO thin films: Optical and electrical properties. AIP Advances 2015, 5, 047143, doi:10.1063/1.4919323.
26. Rehman, S.; Mumtaz, A.; Hasanain, S.K. Size effects on the magnetic and optical properties of CuO nanoparticles. Journal of Nanoparticle Research 2010, 13, 2497-2507, doi:10.1007/s11051-010-0143-8.
27. Schmid, G. Nanoparticles From Theory to Application. 1st edn. Wiley-VCH Verlag GmbH & Co, Weinheim 2004.